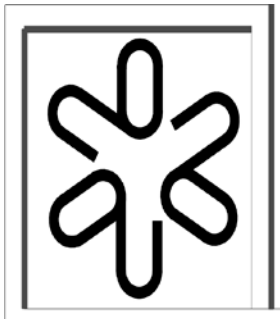

Instituto de Física
Universidade de São Paulo

Determination of the tunneling decay length for nanocomposites Au-PMMA

M. C. Salvadori,
F. S. Teixeira
M. Cattani

Publicação IF 1708
13/03/2018

UNIVERSIDADE DE SÃO PAULO
Instituto de Física
Cidade Universitária
Caixa Postal 66.318
05315-970 - São Paulo - Brasil

Determination of the tunneling decay length for nanocomposites Au-PMMA

M. C. Salvadori[1*], F. S. Teixeira[1], M. Cattani[1]

[1]*Institute of Physics, University of São Paulo, C.P. 66318, CEP 05315-970, São Paulo, S.P., Brazil*

Abstract.

In this work nanocomposites formed by gold ion implantation in PMMA (polymethylmethacrylate), using low energy, are analyzed by transmission electron microscopy, concerning to the nanoparticles size and distribution. Different implantation doses (x) were used and parameters as number of gold nanoparticles per area ρ, diameter distribution $D(x)$ and the distances between the surfaces of the metallic nanoparticles $\delta(x)$, among others parameters, were obtained. It was possible to observe that, as the dose increases, the particles diameter $\overline{D}$ increases, the most probable nearest neighbors distance δ decreases and the number of particles per area ρ also decreases. With the results, it was also possible to calculate the tunneling decay length ξ and the electron affinity ε of the PMMA modified by the gold ion implantation.

Keywords: *Tunneling, Percolation*

---

[*] Corresponding author. Tel.: +55 11 3091 6857; fax: +55 11 3091 6749.

E-mail address: mcsalvadori@if.usp.br (Maria Cecilia Salvadori).

1. Introduction

Nanocomposites formed by metallic nanoparticles in insulator matrix present specific electron transport regimes, accordingly to the amount of metal present in the system. [1] For low concentration of the metallic phase, the system can be described as isolated nanoparticles in an insulator matrix and the electron transport follows the power-law

$$\ln[\sigma(x)] = -\frac{2\delta(x)}{\xi(x)} + const \qquad (1),$$

where σ is the nanocomposite conductivity; x is the metal amount ratio ϕ/ϕ_0, where ϕ_0 is the maximum metal phase for which the system remains a composite. For higher metal concentration, a metallic film starts to be formed and the sample begins to take on the characteristics of a thin metal film; $\delta(x)$ is the average distance between the surfaces of the metallic nanoparticles and $\xi(x)$ the tunneling decay length which depend on the nature of the composite constituents.

For nanocomposites with higher concentration of the metallic phase, [2-4] the nanoparticles start to touch each other until forming a net, when the metal concentration is defined as critical concentration x_c, or percolation threshold, and the electron transport follows the power-law

$$\sigma = \sigma_0(x - x_c)^t \qquad (2),$$

where σ_0 is a saturation conductivity (corresponding to metal amount ϕ_0) and t is the critical exponent.

In a recent paper [4] we have studied the dimensional effects on the tunneling conductivity in nanocomposites obtained by gold ion implantation in PMMA (polymethylmethacrylate) and in alumina. In this previous work, we discussed the two and tridimensionality of the films below the critical concentration x_c of the metallic phase using the "effective-medium approximation" (EMA).[1] In this approximation, we suppose a random distribution of spherical nanoparticles, with diameter D, in an insulator matrix, without measuring the distribution of $D(x)$ and the average distance between the surfaces of the metallic nanoparticles $\delta(x)$. Even so, the results obtained in this paper [4] were consistent for the tunneling decay length $\xi(x)$, validating the EMA approach.

In this paper we worked specifically with nanocomposites Au-PMMA films. These nanocomposites were obtained by gold ion implantation in PMMA, using low energy. It is known that the excess of neutral metallic atoms above the solubility limit of the insulating matrix leads to nucleation and growth of metal nanoparticles.[5] Our approach in this paper was measuring experimentally the nanoparticles diameter distribution $D(x)$ and the distances between the surfaces of the metallic nanoparticles $\delta(x)$, among others parameters, for 3 different doses, using transmission electron microscopy (TEM). In this way, the parameter $\xi(x)$ could be precisely determined using Eq.(1) with our experimental conductivity results.[4] In addition the electron affinity ε of the PMMA modified by the gold ion implantation was also obtained.

2. Materials and Methods

2.1 Preparation of PMMA

PMMA 950k A2 from Microchem Corp. (molecular weight of 950.000 g/mol, with concentration of 2% in anisol solvent) was used to prepare the substrates for gold implantation. The volume of 100 mL was put in a beaker and heated to 120 ºC (above the glassy transition temperature of PMMA T_g ~105°C) during 6 hours to evaporate the solvent. The thickness of the solidified PMMA, after it has cooled down, was approximately 1 mm. Then a tiny piece of about 1mm x 2 mm was cut with a scalpel. This piece was put in a sample holder to make sections of approximately 60nm using the ultramicrotome UC7 from Leica at ambient temperature. The velocity of cutting was 0.4 mm/s. The sections were then fished and put on cooper grids. Each grid hosted about 3 sections. The PMMA sections on grids were the substrates for gold implantation.

2.2 Gold implantation

Gold implantation was carried on using a FCVA (Filtered Cathodic Vacuum Arc) plasma deposition system. In this technique, vastly described in others works,[6-8] a cathode of gold is mounted in a ceramic liner, which in turn is mounted in a hollow anode, forming the plasma gun. A 5 ms arc pulse with current of about 200 A is then established between cathode and anode and cathode spots are formed on the surface of cathode. These high-density spots expand in a plasma. In series with the plasma gun a 90 degrees bent solenoid is mounted and the same arc current flows through it, creating a magnetic field of about 2 mT. This solenoid filters the plasma removing micrometric particles coming from the gun. The plasma then arrives on the substrate with atomic translational energy of about 49 eV.[9] Note that, this energy (49 eV) is the implantation energy considered in this work. The operation frequency of the plasma gun is 1 Hz. The arc pulse rate was determined by depositing a gold film with 1200 pulses in a piece of silicon with an ink mark. The ink was then removed with isopropyl alcohol and the formed step was measured by atomic force microscopy (AFM) to determine the thickness of the film. The average rate was about 0.04 nm/pulse or 10^{14} atoms/cm^2. This average rate was used for planning the number of pulses for each desired gold implantation dose.

Three different doses were implanted on three different grids hosting PMMA sections. Together with each grid, a silicon piece of 10 mm x 10 mm was put to determine afterward the implantation dose through RBS (Rutherford Backscattering Spectrometry). With this procedure, we obtained 3 grids (with 3 sections each) with doses of 0.42 x 10^{16} cm^{-2}, 0.53 x 10^{16} cm^{-2} and 0.80 x 10^{16} cm^{-2}, which corresponds to x of 0.21, 0.26 and 0.40, given the saturation dose of 2 x 10^{16} cm^{-2} determined in our previous work.[4]

2.3 Microscopy and Image Analysis

A Transmission Electron Microscope JEM-2100 from Jeol was used for imaging samples of PMMA implanted with gold. ImageJ (Image Processing and Analysis in Java) package [10] was used to image processing using Fast Fourier Transform (FFT) filtering, thresholding and binarization. Matlab R2015a (Mathworks, Massachusetts) was used to make a routine to determine several features from images, namely: total area analyzed, total number of particles, number of particles per area, particles area percentage coverage, mean of equivalent diameter, the number of interacting pairs considered for measuring the nearest neighbors distances, and most probable value of nearest neighbors distance (mode for a lognormal distribution). The number of analyzed images for each gold dose implantation in PMMA was 6 or 7, taken from the several sections in different grids.

3. Results and Discussion

Typical images of the nanocomposites Au-PMMA obtained by top view TEM are presented in figures 1a, 1b and 1c, with normalized doses of 0.21, 0.26 and 0.40, respectively. It is possible to observe the increase of the nanoparticle size with the dose and, for the higher dose, the nanoparticles start to touch each other.

After processing, the resultant images were binary, as illustrated by figure 2a, corresponding to a TEM image of Au-PMMA with normalized dose of $x = 0.4$. The black pixels refers to the particle and have value 0 and the white pixels have value 1. For obtaining the nearest neighbors all the centroids were determined. Then all particles were connected by straight lines and, for determining if a pair of particles consisted of nearest neighbors, every pixel of the line was scanned between centroids. If there were only two detections of pixel value change (from 0 to 1 and from 1 to 0) the particles were nearest neighbors. Once the pair was detected, from the scanning also the radii r_1 and r_2 along the line were determined, together with the distance d between centroids. Thus, the nearest neighbor distance was determine simply by $\delta = d - (r_1+r_2)$. A number Z of delta measurements was performed generating a map (figure 2b) and a respective histogram (figure 2c). In this way, Z is the number of interacting pairs considered for δ measurements. The histogram of figure 2c consists of a distribution from which the most probable value (mode) could be determined from a lognormal fit (continuous line).

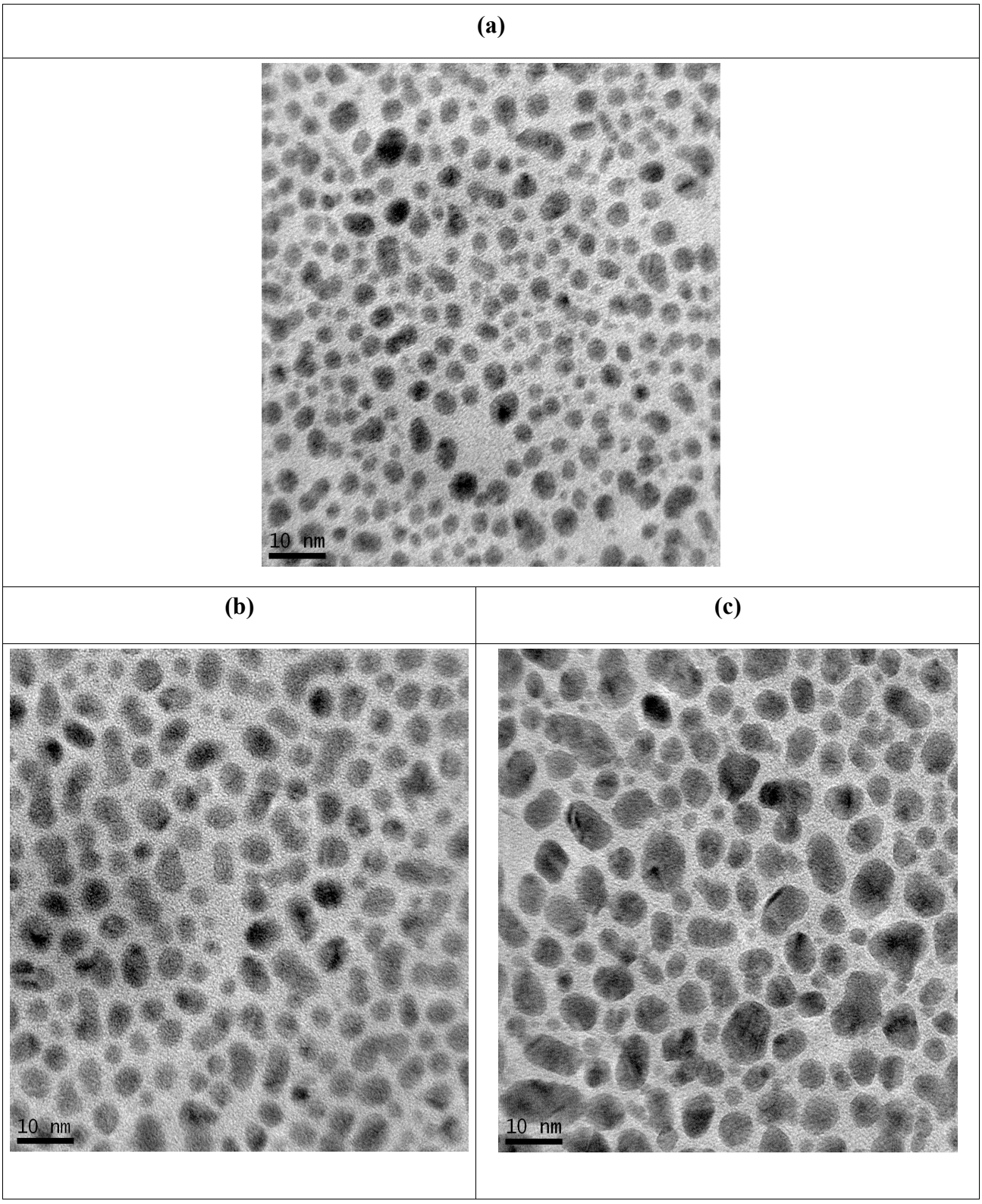

Figure 1- Typical images of top view TEM for the nanocomposites Au-PMMA with normalized doses of (a) $x = 0.21$, (b) $x = 0.26$, (c) $x = 0.40$.

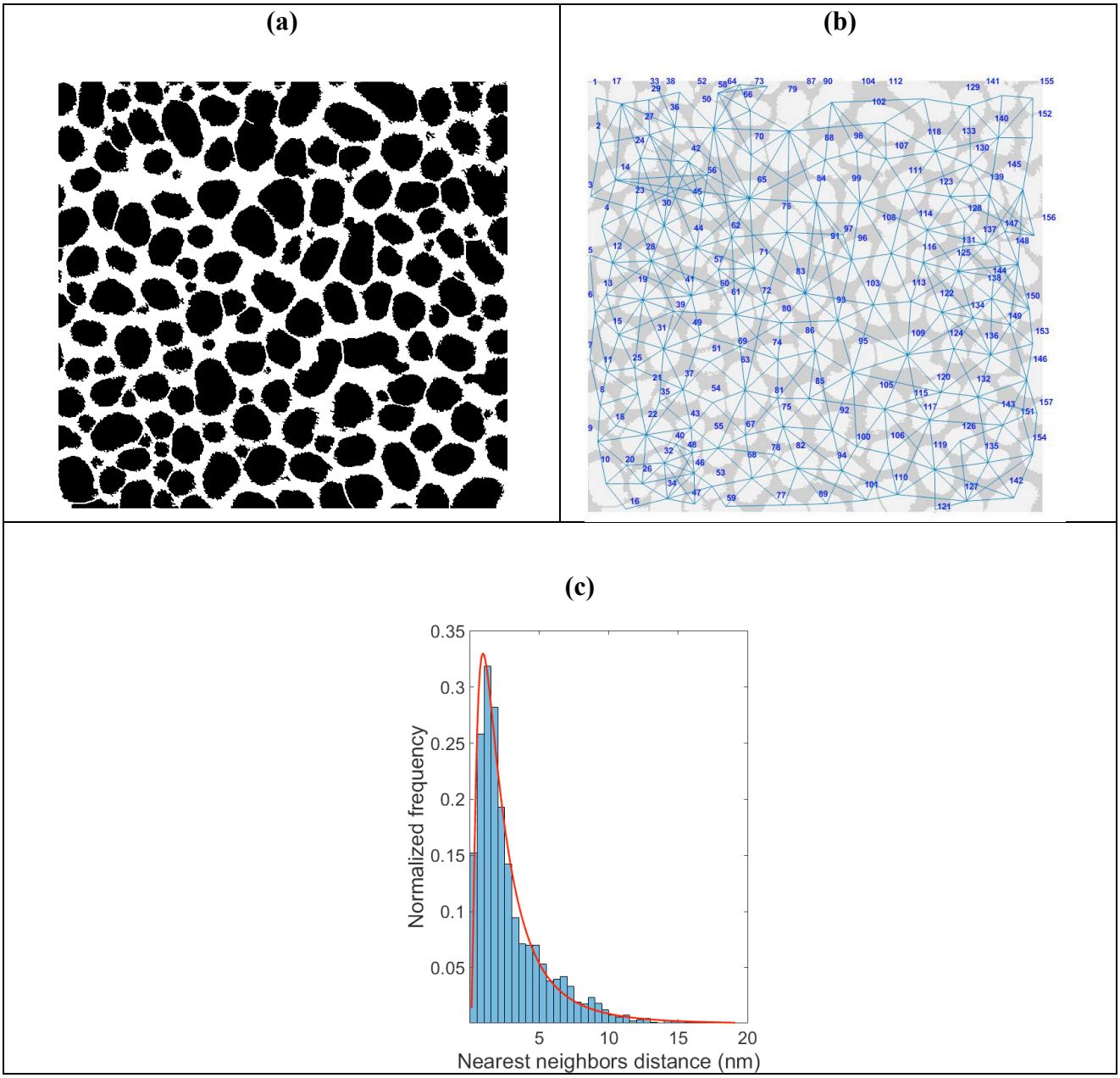

Figure 2 – (a) Representative binary image for TEM image of Au-PMMA with normalized dose of x = 0.40; (b) nearest neighbors map generated for the same image; (c) lognormal of the nearest neighbors distance δ distribution for 7 analyzed images.

Table 1 summarizes all data obtained from the above image analysis: particles area percentage coverage, number of particles per area ρ, mean equivalent particles diameter $\overline{D}$, number of interacting pairs considered for measuring the nearest neighbors distances Z, mode of the nearest neighbors distance δ. The results for x = 0.21, 0.26 and 0.40 are summarized in table 1. It can be observed that, as the dose increases, the particles diameter $\overline{D}$ increases and, consequently, also the particles area percentage coverage increases. On the other way, the most probable nearest neighbors distance decreases δ, that is, the particles are closer to each other. Note that, the number of interacting pairs (Z) considered for measuring the nearest neighbors distances is high (between

~3,500 and ~7,500) allowing reliability for the δ calculation. The number of particles per area ρ also decreases, as the dose increases, suggesting that the nanoparticles are growing and aggregating, consequently generating particles with larger diameters.

Table 1 – Data obtained from the TEM images analysis, where ρ is the number of particles per area, $\bar{D}$ the mean equivalent particles diameter, Z the number of interacting pairs considered for measuring the nearest neighbors distances, δ the mode of the nearest neighbors distance.

	$x = 0.21$	$x = 0.26$	$x = 0.40$
number of analyzed images	6	7	7
total area analyzed [nm^2]	$3.7x10^4$	$4.2x10^4$	$4.3\ x10^4$
particles area percentage coverage	37.2 %	49.1%	59.1 %
ρ [particles/nm^2]	0.052	0.032	0.027
$\bar{D}$ [nm]	2.91 ± 0.05	4.24 ± 0.13	4.99 ± 0.10
Z	7442	4853	3474
δ [nm]	1.53 ± 0.04	1.47 ± 0.04	0.91 ± 0.04

Using Eq.(1) and the conductivity data presented elsewhere[4] and in possession of δ, the tunneling decay length ξ could be calculated. Table 2 shows the ξ values obtained for the samples with x = 0.21, 0.26 and 0.40.

Table 2 – Calculated ξ using Eq. (1)

x	Mean diameter $\bar{D}$ [nm]	Nearest neighbor distance δ [nm]	σ/σ_0	ξ [nm]
0.21	2.91 ± 0.05	1.53 ± 0.04	5.62×10^{-6}	0.25
0.26	4.24 ± 0.13	1.47± 0.04	1.53×10^{-5}	0.26
0.40	4.99 ± 0.10	0.91 ± 0.04	4.19×10^{-4}	0.23

For different implantation doses x, our estimated tunneling decay length ξ are practically the same. This implies that, independently of the gold implantation dose, the PMMA has the same tunneling decay length ξ. Note that, the PMMA hosting the gold nanoparticles is not anymore the original one, it must have an amount of gold diluted on it and also must have broke chain, due to the bombardment of gold ions then, in this case, it is a modified PMMA.

From the tunneling decay length ξ obtained, it is possible to extract one more electrical parameters of this modified PMMA, that is the electron affinity of this material. Taking into account the theoretical estimation of ξ given by[1]

$$\xi = \frac{\hbar}{\sqrt{2m\varphi}}, \qquad (3)$$

where m is the electron mass and φ is the tunnel barrier given by

$$\varphi = W - \varepsilon, \qquad (4)$$

W been the gold work function and ε the electron affinity of the modified PMMA.

In this way, considering the Eq. (3), Eq. (4) and the average tunneling decay length ξ obtained in this work, 0.25 nm, for the nanocomposite Au-PMMA, it is possible to estimate the electron affinity ε of the modified PMMA. The gold work function is $W = 5.4$ eV[11] then, we verify that $\varepsilon = 4.8$ eV, that is about one order of magnitude higher than the electron affinity of the original PMMA[12] $\varepsilon = 0.5$ eV.

4. Summary and Conclusions

Nanocomposites formed by gold ion implantation in PMMA were analyzed by TEM and quantitative characterization was performed. Three implantation doses were analyzed: x = 0.21, 0.26 and 0.40. It was possible to observe that, as the dose increases, the particles diameter $\bar{D}$

increases, the most probable nearest neighbors distance δ decreases and the number of particles per area ρ also decreases. These results suggest that, increasing the dose, the nanoparticles start to grow and aggregate, consequently generating particles with larger diameters and closer to each other.

The most probable nearest neighbors distance δ obtained in this work, for each implantation dose (x = 0.21, 0.26 and 0.40), associated to the conductivity data published previously[4], allowed to calculate the tunneling decay length ξ of the modified PMMA. For the three different x values our estimated tunneling decay lengths ξ are practically the same.

In addition, taking into account the tunneling decay lengths ξ obtained, it was possible to calculate the electron affinity ε of the PMMA modified by the gold ion implantation. The obtained electron affinity of the modified PMMA was ε = 4.8 eV, that is about one order of magnitude higher than the electron affinity of the original PMMA[12] ε = 0.5 eV.

Acknowledgments

This work was supported by the Fundação de Amparo a Pesquisa do Estado de São Paulo (FAPESP), the Conselho Nacional de Desenvolvimento Científico e Tecnológico (CNPq) and Coordenação de Aperfeiçoamento de Pessoal de Nível Superior (CAPES), Brazil. We thank the "Laboratório de Materiais e Feixes Iônicos" of the Institute of Physics, University of São Paulo, for the RBS analysis.

References

[1] C. Grimaldi, Physical Review B 89, 214201 (2014).

[2] M. C. Salvadori, M. Cattani, F. S. Teixeira, I. G. Brown, App. Phys. Lett, 93, 073102 (2008)

[3] F. S.Teixeira, M. C. Salvadori, M. Cattani, S. M. Carneiro, and I. G. Brown, J. Vac. Sci. Technol. B, 27(5), 2242-2247 (2009).

[4] C. Grimaldi, M. Cattani, M. C. Salvadori, J. App. Phys., 117, 125302 (2015).

[5] A. L. Stepanov, D. E. Hole, P. D. Townsend, J. Non-Crystalline Sol 260, 65-74 (1999)

[6] I.G. Brown, Annual Review of Materials Science, (Annual Reviews, Palo Alto, CA, 1998), Vol. 28.

[7] J. Ferreira, F. S. Teixeira, A. R. Zanatta, M. C. Salvadori, R. Gordon, and O. N. Oliveira, Phys. Chem. Chem. Phys., 14(6), 2050-2055 (2012).

[8] F. S.Teixeira, M. C. Salvadori, M. Cattani, S. M. Carneiro, and I. G. Brown, J. Vac. Sci. Technol. B, 27(5), 2242-2247 (2009).

[9]A. Anders, G. Y. Yushkov, J. Appl. Phys, 91(8), (2002)

[10] C.A. Schneider, W. S. Rasband, K. W. Eliceiri. Nat. Methods 9, 671-675 (2012).

[11] H.A.Michelson. JAP 48, 4729(1977).

[12]S. M. Sayyah, A.B.Khaliel and H.Moustafa. International Journal of Polymeric Materials 54:505-518 (2005).